Elastic Analysis of Pavement Structure with Application of Vertical and Centripetal Surface Forces

Maina, J. W.
CSIR Built Environment, Pretoria, South Africa

Fujinami, K. & Matsui, K.
Department of Civil and Environmental Engineering, Tokyo Denki University, Saitama, Japan

Takemi Inoue,
NIPPO Corporation, Tokyo, Japan

ABSTRACT: Contact stresses at the tire/pavement interface for a stationary or rolling wheel comprise not only of vertical stress component but also centripetal stress as well. In this research, wheel load in the form of conically distributed centripetal load and uniformly distributed vertical load were considered and a new development for a closed form solution was introduced. The solution was utilized to analyze a three-layered pavement structure in order to clarify the influence of centripetal load on the pavement responses. Higher tensile stresses at the surface of the pavement along the edge of the load were found. Furthermore, tensile stresses were found at the bottom of the top layer below the centre of the load.

KEY WORDS: Centripetal load, vertical load, linear elastic theory, Hankel transform.

1. INTRODUCTION

Until recently, vertical load only was used in the analysis of pavements. However, several researches have shown existence of complex contact stresses at the tire/pavement interface. According to JRA (2001), in addition to vertical load at the tire/pavement interface, the presence of horizontal, torsional as well as centripetal loads were also reported. While torsional load occurs under certain condition only, vertical, horizontal and centripetal loads were found to act at any time the wheel is stationary or rolling. Up until now, much attention has been focused on the analysis of vertical load only with the assumption that cracking at the bottom of asphalt mixture results from the tensile strain due to action of vertical loading at the pavement surface. However, if pavement cracking is caused by tensile stresses or strains only, then it would be difficult to explain the cause of top-down cracking (Matsuno and Nishizawa 1992, Myers et al. 1998) that has now started to receive a lot of attention and coverage. This paper looks at the centripetal load, which is normally ignored during pavement analysis but forms part of the total wheel load acting on the paper surface.

Several researches have shown existence of forces acting from the tire edge towards the centre of the contact area (Tielking and Roberts, 1987, Barber, 1963, Watanabe, 2002). This type of shear force is what is referred to as centripetal load in this paper and modelling for a load distribution giving a resultant force equal to zero was developed. It has also been reported that contact stresses at the tire/pavement interface are very

complex (De Beer et al. 1997). Blab (1999) developed a model to express stress distribution of the complex contact stresses for use in finite element analysis. But preparation of input data and evaluation of the results from FEM package is time consuming. Furthermore, maintaining high accuracy for responses such as stresses at points of interest is tricky and needs special consideration and technique.

In Japan, the widely used software for pavement analysis are BISAR (De Jong et al. 1979), Chevron, ELSA, GAMES (Matsui et al. 2001, Maina and Matsui, 2004). Chevron and ELSA consider vertical load only as external load, while BISAR and GAMES consider not only vertical load but also horizontal load as external loads. Also, authors have presented the closed form solutions for torsional surface load (Maina et al. 2005) and surface moment load (Maina, et al. 2006). However, authors are not aware of any publication that has dealt with closed form solution for centripetal load acting at the surface of a multilayered pavement system. This paper presents theoretical development of closed form solutions of responses due to the action of centripetal load by directly applying Hankel transform to Navier's equations. This approach is one of the distinctive features of this paper.

2. BOUNDARY CONDITIONS AND GOVERNING EQUATIONS

In axi-symmetric elastic problems, there are displacements u_r, u_z in horizontal, r, and vertical, z, directions, respectively. Stresses will be σ_r, σ_z and σ_θ in the horizontal, r, and vertical, z, and circular, θ, direction, respectively as shown on Figure 1.

According to Tielking and Roberts (1987), the load distribution for a circular centripetal load acting on the pavement surface will be close to conically distributed shape as shown on Figure 2. Taking into consideration this distribution, centripetal load may be modelled such that it is zero at the centre of the contact area ($r = 0$) and maximum, q_0, at the extreme edge of the contact area. When circular vertical and centripetal loads act at the surface of the pavement, the boundary condition may be expressed as follow:

$$\sigma_z(r,0) = \begin{cases} p_0 & (0 \le r \le a) \\ 0 & (r > a) \end{cases} \tag{1a}$$

$$\tau_{rz}(r,0) = \begin{cases} \dfrac{q_0 r}{a} & (0 \le r \le a) \\ 0 & (r > a) \end{cases} \tag{1b}$$

where, a, is the radius of the contact area, whereas Equation (1a) represents boundary conditions for uniformly distributed vertical load while Equation (1b) represents boundary conditions for the centripetal load that is directed from the edge to the centre of the loaded area. The loading distribution was modelled as shown on Figure 3.

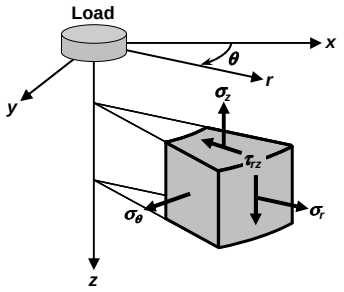

Figure 1: Stresses on an infinitesimal cube in a semi-infinite system.

If z approaches infinity ($z \to \infty$), all responses will be zero:

$$u_r(r,\infty) = u_z(r,\infty) = 0 \tag{2a}$$

$$\sigma_r(r,\infty) = \sigma_\theta(r,\infty) = \sigma_z(r,\infty) = \tau_{rz}(r,\infty) = 0 \tag{2b}$$

The stress-displacement relationship in axi-symmetric problem is as shown below:

$$\sigma_r = (\lambda + 2\mu)\frac{\partial u_r}{\partial r} + \lambda\frac{u_r}{r} + \lambda\frac{\partial u_z}{\partial z} \tag{3a}$$

$$\sigma_\theta = \lambda\frac{\partial u_r}{\partial r} + (\lambda + 2\mu)\frac{u_r}{r} + \lambda\frac{\partial u_z}{\partial z} \tag{3b}$$

$$\sigma_z = \lambda\left(\frac{\partial u_r}{\partial r} + \frac{u_r}{r}\right) + (\lambda + 2\mu)\frac{\partial u_z}{\partial z} \tag{3c}$$

$$\tau_{rz} = \mu\left(\frac{\partial u_r}{\partial z} + \frac{\partial u_z}{\partial r}\right) \tag{3d}$$

where, λ, μ are Lamé constants.

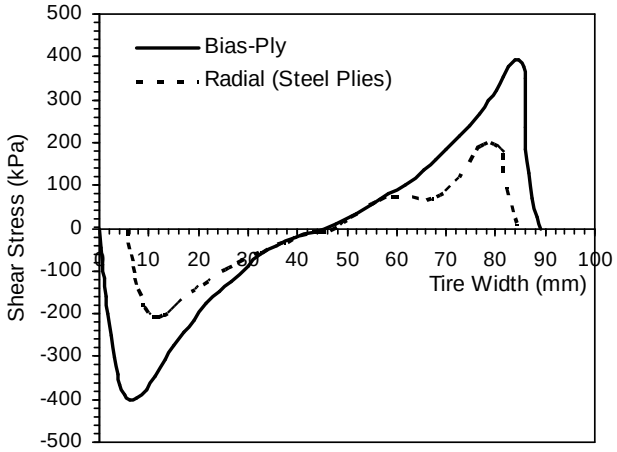

Figure 2: Centripetal tire loads at the surface of a semi-infinity system (Tielking and Roberts, 1987).

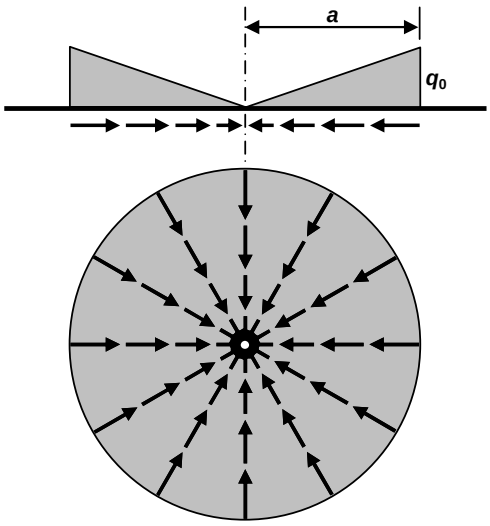

Figure 3: Centripetal load model at the pavement surface.

The equilibrium equations in cylindrical coordinate system may be written as follows:

$$\frac{\partial \sigma_r}{\partial r}+\frac{\partial \tau_{rz}}{\partial z}+\frac{\sigma_r-\sigma_\theta}{r}+F_r=0 \tag{4a}$$

$$\frac{\partial \tau_{rz}}{\partial r}+\frac{\partial \sigma_z}{\partial z}+\frac{\tau_{rz}}{r}+F_z=0 \tag{4b}$$

where, F_r, F_z are body forces in r and z directions, respectively. Assuming body forces to be zero and substitute Equation 3 into Equation 4 to obtain Navier equations for axi-symmetric problems in terms of displacement as follows:

$$(\lambda+2\mu)\left\{\frac{\partial^2 u_r}{\partial r^2}+\frac{1}{r}\frac{\partial u_r}{\partial r}-\frac{1}{r^2}u_r\right\}+(\lambda+\mu)\frac{\partial^2 u_z}{\partial r\partial z}+\mu\frac{\partial^2 u_r}{\partial z^2}=0 \tag{5a}$$

$$(\lambda+\mu)\left(\frac{\partial^2 u_r}{\partial r\partial z}+\frac{1}{r}\frac{\partial u_r}{\partial z}\right)+\mu\left(\frac{\partial^2 u_z}{\partial r^2}+\frac{1}{r}\frac{\partial u_z}{\partial r}\right)+(\lambda+2\mu)\frac{\partial^2 u_z}{\partial z^2}=0 \tag{5b}$$

3. SOLUTIONS FOR THE GOVERNING EQUATIONS

3.1 Semi-infinity system

Hankel transform of the boundary conditions presented in Equation 1 yields:

$$\tilde{\sigma}_z(\xi,0)=\int_0^\infty r\sigma_z(r,0)J_0(\xi r)dr=-p_0\int_0^a rJ_0(\xi r)dr=-\frac{p_0 a}{\xi}J_1(\xi a) \tag{6a}$$

$$\tilde{\tau}_{rz}(\xi,0)=\int_0^\infty r\tau_{rz}(r,0)J_1(\xi r)dr=\frac{q_1}{a}\int_0^a r^2 J_1(\xi r)dr=\frac{q_1 a}{\xi}J_2(\xi a) \tag{6b}$$

where J_0, J_1, and J_2 are Bessel functions of type one and 0, 1 and 2 orders, respectively.

Performing Hankel transform on the Navier equations and rearrange to obtain Equation 7 as follows:

$$\left(\frac{d^2}{dz^2}-\frac{(\lambda+2\mu)}{\mu}\xi^2\right)\tilde{u}_r(\xi,z)-\frac{(\lambda+\mu)}{\mu}\xi\frac{d}{dz}\tilde{u}_z(\xi,z)=0 \tag{7a}$$

$$\frac{(\lambda+\mu)}{\mu}\xi\frac{d}{dz}\tilde{u}_r(\xi,z)+\left\{\frac{(\lambda+2\mu)}{\mu}\frac{d^2}{dz^2}-\xi^2\right\}\tilde{u}_z(\xi,z)=0 \tag{7b}$$

where,

$$\tilde{u}_r(\xi,z)=\int_0^\infty ru_r(r,z)J_1(\xi r)dr \tag{8a}$$

$$\tilde{u}_z(\xi,z)=\int_0^\infty ru_z(r,z)J_0(\xi r)dr \tag{8b}$$

Cancel $\tilde{u}_r(\xi,z)$ from Equation (7) to obtain:

$$\frac{\lambda+2\mu}{\mu}\left(\frac{d^2}{dz^2}-\xi^2\right)^2\tilde{u}_z(z,\xi)=0 \tag{9}$$

This gives:

$$\tilde{u}_z(\xi,z)=\{A(\xi)+B(\xi)z\}e^{-\xi z}+\{C(\xi)+D(\xi)z\}e^{\xi z} \tag{10}$$

Equation (11) represents the relationship between Lamé constants and Poisson's ratio:

$$\lambda=\frac{2\nu}{1-2\nu}\mu \tag{11}$$

Substituting Equation (10) into Equation (7b) to obtain:

$$\tilde{u}_r(\xi,z)=\left\{A-\frac{3-4\nu-\xi z}{\xi}B\right\}e^{-\xi z}-\left\{C+\frac{3-4\nu+\xi z}{\xi}D\right\}e^{\xi z} \tag{12}$$

Then, on performing Hankel transform of Equation (3c) and substitute Equations (10)~(12) and rearrange, yields:

$$\tilde{\sigma}_z=\int_0^\infty r\,\sigma_z J_0(\xi r)dr=2\mu\{-\xi A+(1-2\nu-\xi z)B\}e^{-\xi z}+2\mu\{\xi C+(1-2\nu+\xi z)D\}e^{\xi z} \tag{13}$$

Similarly, performing Hankel transform on Equation (3d) and substitute Equations (10)~(12) and rearrange to obtain:

$$\tilde{\tau}_{rz}=\int_0^\infty r\,\tau_{rz}\,J_1(\xi r)dr=-2\mu\{\xi A-(2-2\nu-\xi z)B\}e^{-\xi z}-2\mu\{\xi C+(2-2\nu+\xi z)D\}e^{\xi z} \tag{14}$$

Rearranging Equations (10), (12), (13), and (14) and express in Matrix form as follows:

$$\begin{Bmatrix}\tilde{u}_r(z,\xi)\\ \tilde{u}_z(z,\xi)\\ \tilde{\sigma}_z(z,\xi)\\ \tilde{\tau}_{rz}(z,\xi)\end{Bmatrix}=[P_1]\begin{Bmatrix}A(\xi)\\ B(\xi)\\ C(\xi)\\ D(\xi)\end{Bmatrix} \tag{15}$$

where $[P_1]$ is a 4×4 matrix whose elements are as shown in Table 1. Furthermore, *A*, *B*, *C*, and *D* are coefficients of integration that may be determined by using the boundary conditions.

In order to determine σ_r, σ_θ, the following Hankel transform is performed.

$$H_1(z,\xi)=\int_0^\infty r(\sigma_r+\frac{2\mu u_r}{r})J_0(\xi r)dr \tag{16a}$$

$$H_2(z,\xi)=\int_0^\infty r(\sigma_r+\sigma_\theta)J_0(\xi r)dr \tag{16b}$$

Substituting Equations (3a,b) into Equation (16), yields:

$$\begin{Bmatrix}H_1(z,\xi)\\ H_2(z,\xi)\end{Bmatrix}=[P_2]\begin{Bmatrix}A(\xi)\\ B(\xi)\\ C(\xi)\\ D(\xi)\end{Bmatrix} \tag{17}$$

where $[P_2]$ is a 2×4 matrix whose elements are as shown in Table 2.

When $z\to\infty$, all responses will be equal to zero and for that to be true then *C*=*D*=0. Consequently, applying boundary conditions expressed in Equation (6) into Equation (15), yields:

$$\begin{Bmatrix}\tilde{\sigma}_z(0,\xi)\\ \tilde{\tau}_{rz}(0,\xi)\end{Bmatrix}=\begin{bmatrix}-2\mu\xi e^{-\xi z} & 2\mu(1-2\nu-\xi z)e^{-\xi z}\\ -2\mu\xi e^{-\xi z} & 2\mu(2-2\nu-\xi z)e^{-\xi z}\end{bmatrix}\begin{Bmatrix}A(\xi)\\ B(\xi)\end{Bmatrix} \tag{18}$$

Solving the above equation gives:

$$A(\xi)=\frac{2(-1+\nu)\tilde{\sigma}_z(0,\xi)+(1-2\nu)\tilde{\tau}_{rz}(0,\xi)}{2\mu\xi} \tag{19a}$$

$$B(\xi)=\frac{-\tilde{\sigma}_z(0,\xi)+\tilde{\tau}_{rz}(0,\xi)}{2\mu} \tag{19b}$$

Responses for a semi-infinity system may be obtained by substituting Equation (19) and *C*=*D*=0 into Equation (15) and perform Hankel inverse transform on the resulting $\tilde{u}_r,\tilde{u}_z,\tilde{\sigma}_z,\tilde{\tau}_{rz}$.

$$u_r = \int_0^\infty \xi \tilde{u}_r J_1(\xi r) d\xi \tag{20}$$

$$u_z = \int_0^\infty \xi \tilde{u}_z J_0(\xi r) d\xi \tag{21}$$

$$\sigma_z = \int_0^\infty \xi \tilde{\sigma}_z J_0(\xi r) d\xi \tag{22}$$

$$\tau_{rz} = \int_0^\infty \xi \tilde{\tau}_{rz} J_1(\xi r) d\xi \tag{23}$$

Furthermore, from Equations (16) and (17):

$$\sigma_r = -\frac{2\mu}{r} u_r + \int_0^\infty \xi [H_1(z,\xi)] J_0(\xi r) d\xi \tag{24}$$

$$\sigma_\theta = -\sigma_r + \int_0^\infty \xi [H_2(z,\xi)] J_0(\xi r) d\xi \tag{25}$$

Extension of the solutions to multilayered system is explained in detailed in the paper published by some of the authors (Maina and Matsui, 2004).

4. WORKED EXAMPLE

4.1 Three-Layer system

Figure 4 shows a three-layer system with the first layer 10cm, second layer 30cm and third layer is semi-infinity. Young's moduli for the three layers are E_1=4,000MPa, E_2=300MPa and E_3=80MPa. Poisson's ratio for all the layers is 0.35. A 15cm radius load is assumed to act at the surface. The load types are a 49kN uniformly distributed vertical load with a pressure of p_0=0.694MPa and a conically distributed centripetal load with edge pressure of q_0=0.694MPa. The purpose is to investigate the influence of centripetal load on the responses. The following analysis was performed. 1) analysis for vertical load only, 2) analysis for centripetal load only and 3) analysis for simultaneous action of vertical and horizontal loads.

Figure 5 shows comparisons of the variation, in the horizontal direction, of $\sigma_r, \sigma_\theta, \sigma_z$ and τ_{rz} at the surface of the first layer for the three types of load cases that were analyzed. Figure 6 shows comparisons of normal stresses at the bottom of the first layer.

σ_r (Figure 5(a)) shows an existence of very high tensile stress near r = 15cm due to centripetal loading but tensile surface stresses decreases considerably when vertical loading is also considered. At r = 0cm, σ_r is compressive and due to the effect of centripetal loading, there is an increase in the compressive stress by about 60%. Even though σ_θ from centripetal load is slightly tensile at the surface where r = 15cm (see Figure 5 (b)), superposition with results from vertical load gives compressive stresses all across the surface. The compressive stress is maximum at r = 0cm, which is an increase

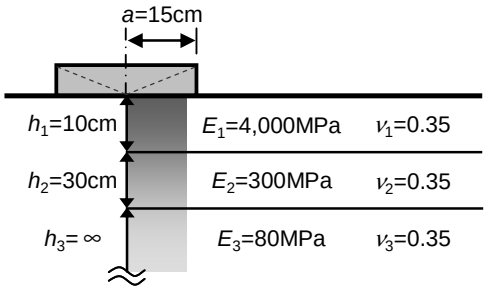

Figure 4: Three-layered pavement model.

of about 60% compared to the results from vertical load only. For the case of centripetal load, σ_z, is zero at the surface, whereas σ_z matches well with the external pressure from the vertical load (see Figure 5 (c)). Figure 5(d) shows variation of τ_{rz} at the surface. Under vertical load, τ_{rz} is zero and the result for centripetal load matches well with the external shear stress.

Both vertical and centripetal loads result in tensile stresses (σ_θ and σ_r) at the bottom of the first layer (Figures 6(a) and 6(b)) and the total stress below the centre of the load is 1.81MPa, which shows the influence of centripetal loading is about 20% of the vertical loading for these two stresses.

σ_z at the bottom of the first layer (Figure 6(c)) is compressive with the value of 0.36MPa, which is about 22% higher than σ_z from vertical load only.

From the results presented above, it was found that the influence of centripetal loading on pavement responses is limited to the neighbourhood of the loaded area.

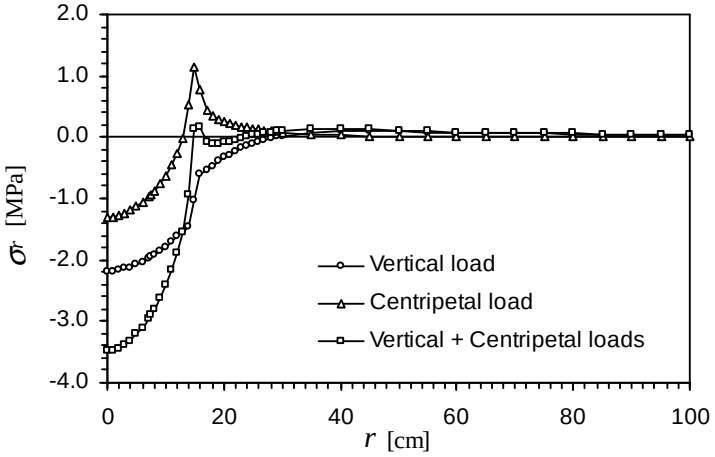

(a) σ_r (surface of first layer)

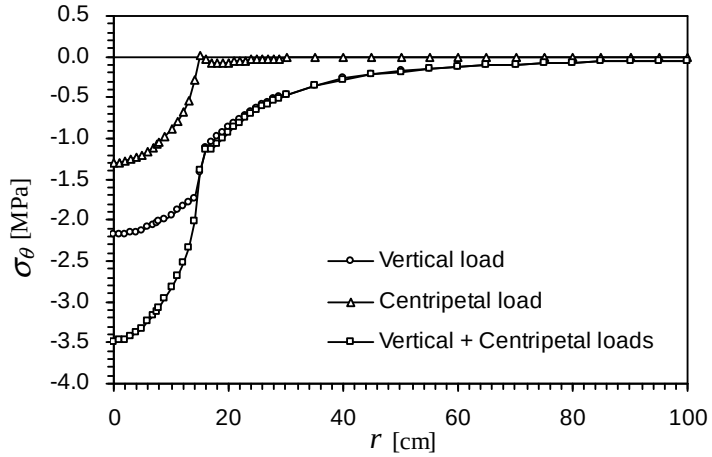

(b) σ_θ (surface of first layer)

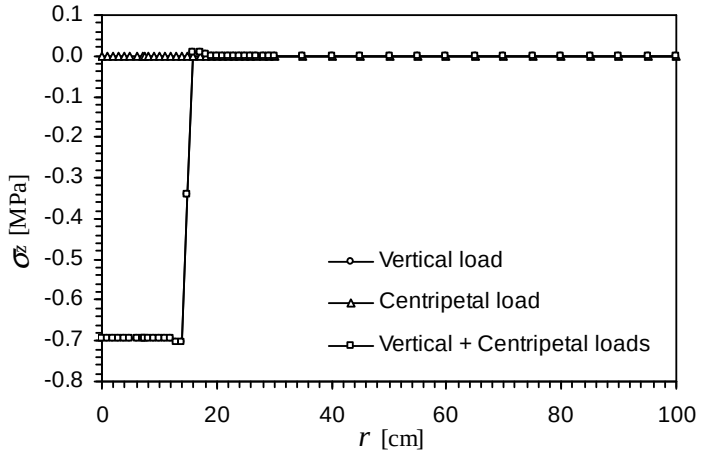

(c) σ_z (surface of first layer)

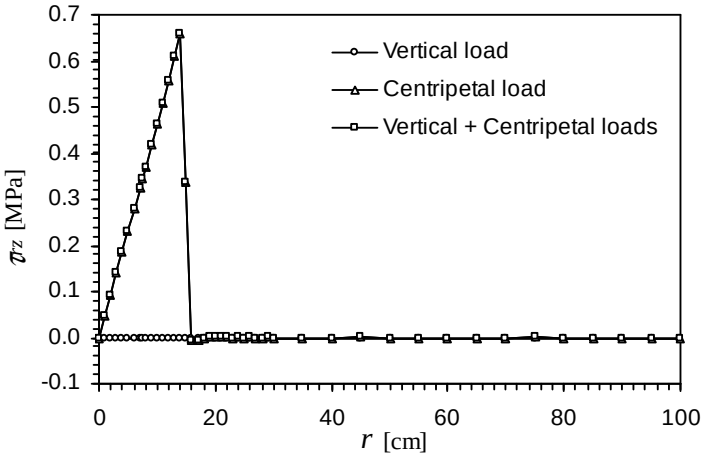

(d) τ_{rz} (surface of first layer)

Figure 5: Normal and shear stresses at the surface of first layer.

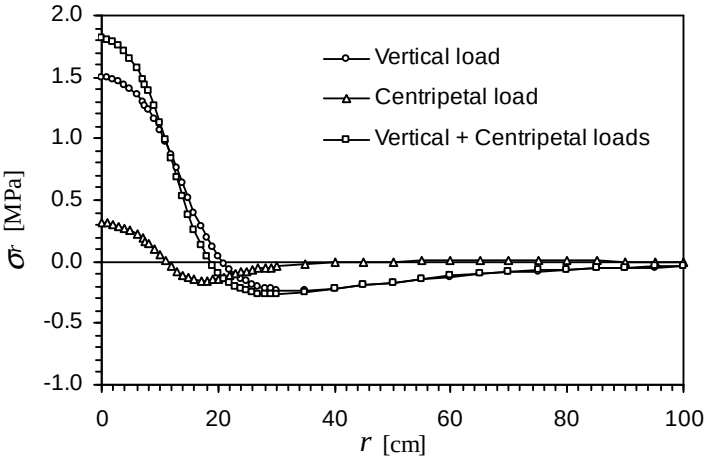

(a) σ_r (bottom of first layer)

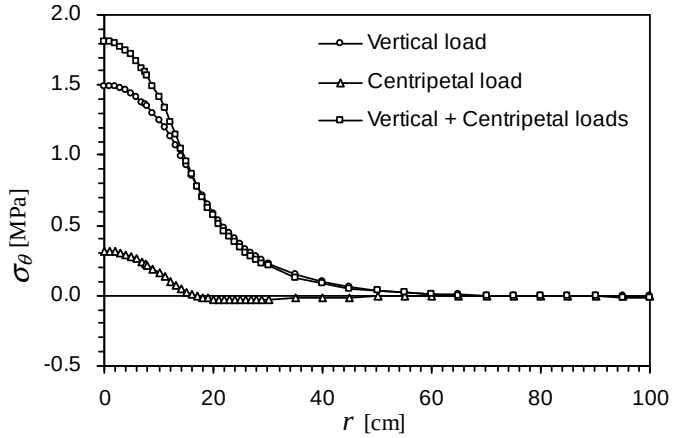

(b) σ_θ (bottom of first layer)

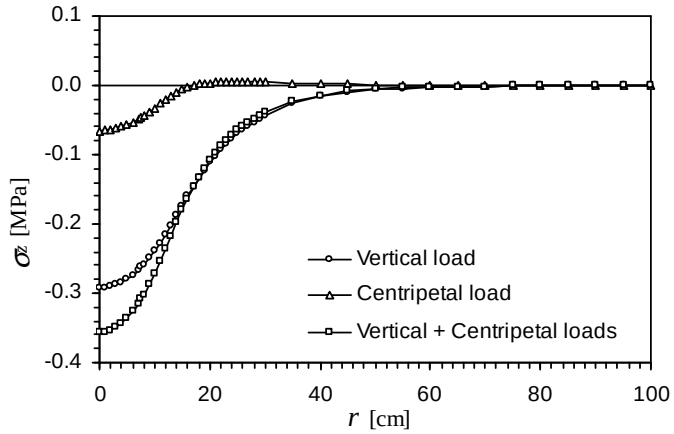

(c) σ_z (bottom of first layer)

Figure 6: Normal stress at the bottom of first layer.

5. OBSERVATIONS AND CONCLUSIONS

In this research, development of closed form solutions for centripetal loading was presented using direct Hankel transform of Navier equations instead of the classic approach, which uses Michell displacement functions. Both approaches were found to give similar results although the shapes of equations are different. Maintaining high level of computational accuracy, especially, near the surface is very difficult and most software, like BISAR (De Jong et al. 1979), devised some modifications to improve the accuracy. This research does not employ any of those strategies because of the robustness of the numerical algorithms used. Results obtained have matched well the external boundary conditions, which is an indication of the level of accuracy of the software (GAMES) developed. The following conclusions were drawn from the results obtained.

1) Tensile stress, σ_r, resulting from the action of centripetal load only is very high along the edge of the loaded area(r = 15cm), but this effect is cancelled out by higher compressive stresses from the vertical load.

2) At the surface of the first layer, the compressive stresses σ_r and σ_θ attained their maximum values when r = 0cm, and the influence of centripetal load was about 60%.

Furthermore, at the bottom of the first layer, both σ_r and σ_θ were tensile and the contribution of centripetal load was found to be about 20%.

3) When r > 30cm the influence of centripetal load becomes negligible. This is an indication that the influence of centripetal load is highly concentrated in the neighbourhood of the loaded area.

In light of the analytical development presented in this paper, future research plan would be: 1) to look at how nonlinear temperature distribution in the asphalt mix influences the results, 2) to consider tire/pavement contact stresses in the analysis and 3) to consider evaluation of factors other than maximum stress for use to improve standards for fatigue failure.

REFERENCES

Barber, E.S. , 1963. Shear Loads on Pavements. *Public Roads, Journal of Highway Research*, Vol.32, No.6, pp.141-144.

Blab, R., 1999. Introducing Improved Loading Assumptions into Analytical Pavement Models Based on Measured Contact Stresses of Tires. *International Conference on Accelerated Pavement Testing*, Reno, NV.

De Beer, M., Fisher, C. and Jooste, F. J., 1997. Determination of Pneumatic Tyre/Pavement Interface Contact Stresses under Moving Loads and Some Effects on Pavements with Thin Asphalt Surfacing Layers. *8th International Conference on Asphalt Pavements*, Seattle Washington, Vol.1, pp.179-227.

De Jong, D.L., Peatz, M.G.F. and Korswagen, A.R., 1979. Computer program BISAR layered systems under normal and tangential surface loads. *External Report* AMSR.0006.73, Koninklijke/Shell-Laboratorium, Amsterdam.

Maina, J.W., Fujinami, K., Matsui, K. and Inoue, T. Mulitilayered elastic Analysis for Surface Moment Loading, Transportation Research Board, 2006 (to be presented).

Maina, J.W., Fujinami, K., Matsui, K. and Inoue, T. Pavement Responses due to Torsional Surface Loading, Proceedings of 7th International Conference on Bearing Capacity of Roads, Railways and Airfields, NTNU, Trondheim, Norway, June 2005.

Maina, J. W. and Matsui, K., 2004. Developing Software for Elastic Analysis of Pavement Structure Responses to Vertical and Horizontal Surface Loadings. *Transportation Research Records*, No. 1896, pp. 107-118.

Matsui, K., Maina, J.W., and Inoue, T., 2002. Axi-symmetric Analysis of Elastic Multilayer System Considering Interface Slips. *International Jouranl of Pavements*, Vol. 1 No. 1, pp. 55-66.

Matsuno, S, and Nishizawa, T.1992. Mechanism of Longitudinal Surface Cracking of Asphalt Pavements, Proceedings 7th International Conference on Asphalt Pavements, Vol.2., pp.277-291.

Myers, L.A., Roque R. and Ruth, B.E., 1998. Mechanism of Surface-Initiated Longitudinal Wheel Path Cracks in High-Type Bituminous Pavements. *Journal of the Association of Asphalt Paving Technologists*, Vol.67.

Tielking, J.T. and Roberts, F.L., 1987. Tire Contact Pressure and Its Effect on Pavement Strain. *Journal of Transportation Engineering, ASCE*, Vol.113, No.1, pp.56-71.

Watanabe T., 2002. Tire Talks. Revised Version, Japanese Standards Association (JSA), Japan. (Japanese)

Working Group for Pavement Technology Standards, 2001. *Revision of Guideline for Design of Pavements under the Action of Special Types of Loads (Design of Pavement Junctions)*. Journal of Road Construction, JRCA, pp. 44-54. (Japanese)